Tribocorrosion behaviour of hot pressed CoCrMo−Al_2O_3 composites for biomedical applications

Z. Doni[1,2], A. C. Alves[1], F. Toptan*[1,3], A. M. Pinto[1,3], L. A. Rocha[1,4], M. Buciumeanu[2], L. Palaghian[2] and F. S. Silva[1,3]

Alumina/alumina wear couple can lower the wear rates and thus metallic ion releasing on load bearing metallic implant materials. However, the low fracture toughness of ceramics is still a major concern. Therefore, the present study aims to process and to triboelectrochemically characterise the 5 and 10 vol.-%Al_2O_3 reinforced CoCrMo matrix composites. Corrosion and tribocorrosion behaviour of the composites were investigated in 8 g L^{-1} NaCl solution at body temperature. Corroded and worn surfaces were investigated by a field emission gun scanning electron microscope equipped with energy dispersive X-ray spectroscopy. After tribocorrosion experiments, wear rates were calculated using a profilometer. Results suggest that Al_2O_3 particle addition decreased the tendency of CoCrMo alloy to corrosion under both static and tribocorrosion conditions. However, no significant influence on the corrosion and wear rates was observed in composites mainly due to increased porosity and insufficient matrix/reinforcement bonding.

Keywords: Al_2O_3, CoCrMo, Composite, Corrosion, Hot pressing, Tribocorrosion

Introduction

Implant materials are subjected to the relative movements, which can cause wear damage, together with the corrosive attack of the body fluids.[1,2] This combined action of wear and corrosion is defined as tribocorrosion, being estimated that in hip implant systems, 20–30% of the material losses can be attributed to corrosion related damage through wear induced/enhanced corrosion process.[3,4]

Co based alloys are widely used for load bearing and articulating orthopaedic implants.[5–8] Even though among all implant materials, CoCrMo alloys exhibit the most useful balance in strength, fatigue and wear, together with corrosion resistance,[9] wear debris generation and metallic ion releasing are still a major concern for CoCrMo implant materials.[10–13] It has been reported that the wear and corrosion products that are generated locally by the implant interfaces may lead to periprosthetic inflammation and implant loosening.[10,14] Besides, released metallic ions from the implant material may become clinically significant over the time, which may result in allergic reactions as well as contribute to implant failure and osteolysis.[11]

It has been suggested that Al_2O_3 coatings may be a solution to minimise problems related to wear debris and metallic ion release. Even though Al_2O_3−ultrahigh molecular weight polyethylene bearing couples are reported to reduce the wear by at least a factor of 2 as compared to the standard CoCr femoral heads, wear rates for Al_2O_3−Al_2O_3 bearing couples can lower the wear rates more than 50 times when compared to the standard CoCr−ultrahigh molecular weight polyethylene couples. However, the low fracture toughness of ceramics is a major concern since even a slow crack growth under stresses well below their fracture strength may be a risk of catastrophic bearing failure in implant materials.[10]

It is well known that problems related to the low fracture toughness of the monolithic ceramics can be overcome using composite materials.[15] Composite structures can also be used to produce functionally graded materials that can eliminate the problems related to the sharp interface transitions found in coatings.[16] However, there is very limited information on Co based composite structures for biomedical applications.

Grądzka-Dahlke *et al.*[17] studied the mechanical and tribological properties of CoCrMo based, calcium pyrophosphate, boron carbide and silicon nitride reinforced composite materials and reported that CoCrMo based composites can be the alternative

[1]Centre for Mechanics and Materials Technologies (CT2M), Universidade do Minho, Azurém, Guimarães 4800-058, Portugal
[2]Faculty of Mechanical Engineering, 'Dunarea de Jos' University of Galati, Galati, Romania
[3]Universidade do Minho, Dept. Eng. Mecânica, Azurém, Guimarães 4800-058, Portugal
[4]Faculdade de Ciências de Bauru, Dep. Física, Univ. Estadual Paulista (UNESP), Bauru, São Paulo 17033-360, Brazil

*Corresponding author, email ftoptan@dem.uminho.pt

Received 2 March 2014; accepted 28 May 2014
DOI 10.1179/1751584X14Y.0000000078

materials for biomedical applications since they offer increased mechanical properties and corrosion resistance. Oksiuta *et al.*[18] studied the structural, mechanical properties and corrosion behaviour of CoCrMo based, 5, 10 and 15 wt-% bioactive glass reinforced composites and reported that, even though ultimate compressing strength and elastic properties of the composites were decreased with increasing amount of the bioglass addition, composites exhibited better corrosion properties as compared to the base alloy. However, while several works were performed on the tribocorrosion behaviour of cast and hot pressed (HP) CoCrMo alloy,[7,19–27] tribocorrosion behaviour of CoCrMo based composites is yet to be studied.

Reinforcing metallic materials with ceramic particles may improve the tribocorrosion behaviour of metal matrix composites (MMCs) by the load carrying effect of the reinforcing particles.[28] However, if the matrix/reinforcement bonding is weak, and the reinforcing particles are not strong enough to withstand the loads, reinforcing particles may be detached or fragmented under the sliding, which may result in even worse wear behaviour as compared to the unreinforced alloy due to the third body effect of the particles.[29] Therefore, the present study aims to investigate the corrosion and tribocorrosion behaviour of 5 and 10 vol.-%Al_2O_3 reinforced HP CoCrMo matrix composites in comparison with its base alloy in 8 g L^{-1} NaCl solution, as a first approach to understand the triboelectrochemical behaviour of the homogeneous outmost layers of a CoCrMo−Al_2O_3 functionally graded materials for implant applications.

Experimental

Materials

Hot pressed CoCrMo and its composites reinforced by 5 and 10 vol.-%Al_2O_3 were produced using CoCrMo (Nobilmetal, Nobil 4000, Villafranca d'Asti, Italy) and Al_2O_3 (Goodfellow) particles both in spherical shape. The chemical composition of the CoCrMo powder is given in Table 1, and the particle size distributions of both CoCrMo and Al_2O_3 powders (obtained by a laser particle analyser, Malvern Series 2600) are given in Table 2.

Processing

Before the processing, Al_2O_3 powders were cleaned with a solution of two acids (1HF:1HNO_3) in order to obtain a better physical contact with the matrix powders. After cleaning, CoCrMo and Al_2O_3 powders were mixed using a ball mill rotating at 80 rev min^{-1} for 3 h and dried in a muffle furnace at 105°C, for 1 h in order to remove the humidity. The samples were produced by hot pressing at 1000°C under vacuum (0·01 mbar) and at a constant pressure (40 MPa) with a sintering time of 30 min. The details of the processing procedure is explained elsewhere.[27]

Before each test, the samples were ground down to 4000 mesh size SiC paper followed by polishing with diamond paste down to 1 μm. After polishing, samples were ultrasonically cleaned in propanol for 10 min followed by distilled water during 5 min. The samples were kept in a desiccator for 24 h before starting the tests in order to obtain the similar surface conditions.

Physical characterisation

The porosity content was determined by metallographic image analysis technique using Leica DM2500 OM and Image J 1·37v image analysis software. Vickers hardness was evaluated as a mean of five indentations per sample using an Officine Galileo Mod. D 200 tester at a load of 30 kg with dwelling time of 20 s.

Corrosion tests

Open circuit potential (OCP) and cyclic polarisation measurements were performed in a 8 g L^{-1} NaCl solution at body temperature (37±2°C) using Gamry potentiostat/galvanostat (model Reference-600). Before the tests, the pH values of the electrolyte were measured through a pH meter (EUTECH Instruments pH 510) as 5·72±0·04 at 37°C. A standard three-electrode electrochemical cell (adapted from ASTM G3-89) with an electrolyte volume of 200 mL was used for the measurements, where saturated calomel electrode (SCE) was used as the reference electrode, Pt electrode was used as the counter electrode and the samples having an exposed area of 0·38 cm^2 was used as the working electrode. Cyclic polarisations were performed using an initial delay time of 60 min in order to stabilise the surface at OCP. A polarisation scan was carried out in the anodic direction, starting at 0·25 V(SCE) more negative than (E_{OCP}), at a rate of 0·5 mV s^{-1}. The sweep direction was reversed at 1 V(SCE).

Tribocorrosion tests

For the tribocorrosion tests, the electrochemical cell was installed on a ball on plate tribometer (CETR-UMT-2) with the working surface of the samples facing upwards, against the counter material. The electrochemical measurements were carried out at 37±2°C using the same three-electrode set-up, together with the same equipment and 30 mL of the same electrolyte (8 g L^{-1} NaCl) used in corrosion tests. Since the work aims at comparing tribocorrosion behaviour of three different samples, measurement of corrosion potential is chosen as a triboelectrochemical technique owing to its simplicity for gathering information on the surface state of the sliding metals.[30] Thus, OCP was measured before, during and after sliding where the sliding action started after 1 h of immersion in order to obtain the stable OCP values. After stabilisation, a 10 mm diameter alumina ball (Goodfellow) was loaded and the sliding applied in a reciprocating system with total stroke length of 3 mm, frequency of 1 Hz, normal load of 1 N and total sliding time of 30 min.

After tribocorrosion tests, samples were ultrasonically cleaned in propanol for 10 min followed by distilled

Table 1 Chemical compositions of CoCrMo powders (from supplier's datasheet)

Element	Co	Cr	Mo	Si	Mn	Ni	C
wt-%	Balance	28·0–30·0	5·0–6·0	Trace	Trace	Trace	Trace

Table 2 Particle size distribution

Particle size distribution/μm	*D*[v,0·1]	*D*[v,0·5]	*D*[v,0·9]
CoCrMo	5·38	9·61	17·16
Al_2O_3	11·16	30·21	53·59

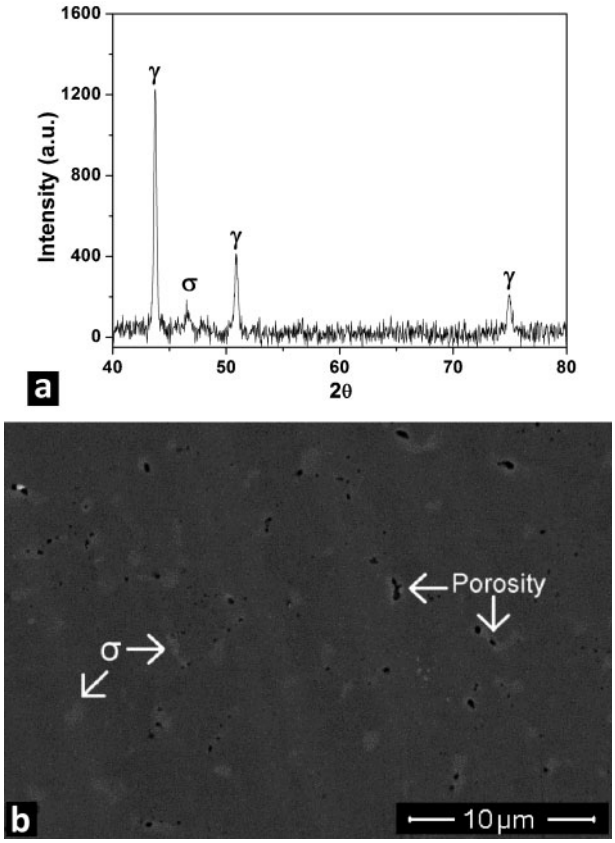

1 *a* X-ray diffraction spectrum and *b* BSE image of HP CoCrMo alloy

water during 5 min. The width and the deepness of the wear tracks were measured by a contact profilometer (Mitutoyo Surftest SJ-500), and the wear rates were calculated by the procedure that is explained elsewhere.[27]

Chemical and microstructural characterisation

Phase analysis of the as processed CoCrMo alloy was carried out by X-ray diffraction using a Bruker D8 DISCOVER diffractometer equipped with a Cu K_α radiation source. As processed microstructures were characterised under a Leica DM2500 optical microscope (OM) and a Nano FEI Nova 200 field emission gun scanning electron microscope equipped with an energy dispersive spectrometer (EDS). Corroded surfaces after corrosion tests and worn surfaces after tribocorrosion tests were also characterised using a field emission gun scanning electron microscope/EDS. All worn surface micrographs were taken as parallel to the sliding direction.

Results and discussion

Microstructure and physical properties

The X-ray diffraction spectrum obtained from HP CoCrMo alloy (unreinforced material) is given in Fig. 1*a*. It has been reported that Co based alloys exhibit a α-fcc metastable matrix due to the slow rate of the fcc→hcp transformation.[31] As can be seen on the spectrum, γ (fcc) phase was obtained as the matrix phase of the alloy. Besides, σ phase was identified with data available for σ-CrCo.[32,33] Those phases can be seen on the SEM image given in Fig. 1*b*.

It is well known that homogeneous particle distribution should be obtained in MMCs in order to achieve the desired properties.[34] As can be seen on the low magnification OM images on Fig. 2, relatively homogeneous particle distribution was observed on HP CoCrMo–Al_2O_3 composites. However, as Al_2O_3 particle content increased, porosity increased and hardness values decreased as shown in Table 3. Since solid diffusion is one of the most important phenomenon that controls the powder metallurgy based processing routes, porosity may increase with the increased volume fraction of inert ceramic reinforcement phase.[35–37] It is well known that, in MMCs, hard reinforcement phase carries much of the applied load, and therefore, hardness increases as compared to the unreinforced matrix.[38] However, in case of presence of porosity, the expected hardness values could not be obtained or even decreased.[39]

Corrosion behaviour

The representative cyclic polarisation curves of the base CoCrMo alloy and the composite samples in 8 g L^{-1} NaCl solution at body temperature are given in Fig. 3. On the forward scan, the base CoCrMo alloy presented a direct translation from the Tafel region to a passivation plateau having a range of 277 ± 11 mV at $i_{pass} = (3{\cdot}53 \pm 0{\cdot}09) \times 10^{-6}$ A cm^{-2}, with starting potential $\sim 21 \pm 8$ mV due to the formation an oxide film on the alloy surface.[40,41] However, passive plateau was not observed for the composite samples, which represented gradually increased anodic current densities. Above a potential of ~645 mV, all samples presented similar behaviour on the polarisation curves.

Corrosion potential and current density values were calculated by Tafel extrapolation method, and the results are given in Table 4. As can be seen from the values, corrosion potential $E_{(i=0)}$ values were decreased by Al_2O_3 particle addition. This behaviour can be explained by the diminished exposed surface area after incorporation of inert Al_2O_3 particles, which shift the

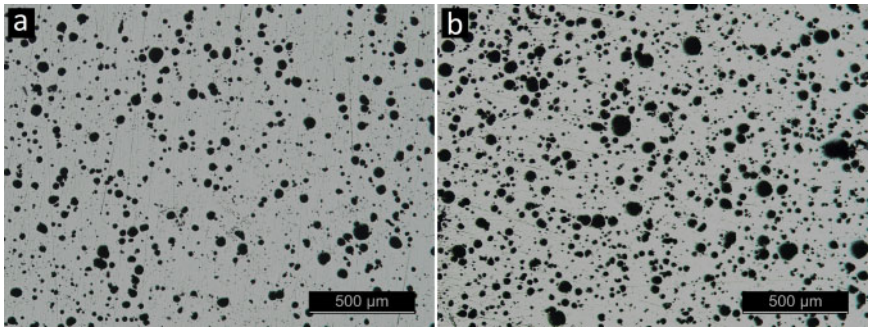

2 Optical microscope images of *a* CoCrMo–5Al_2O_3 and *b* CoCrMo–10Al_2O_3 composites

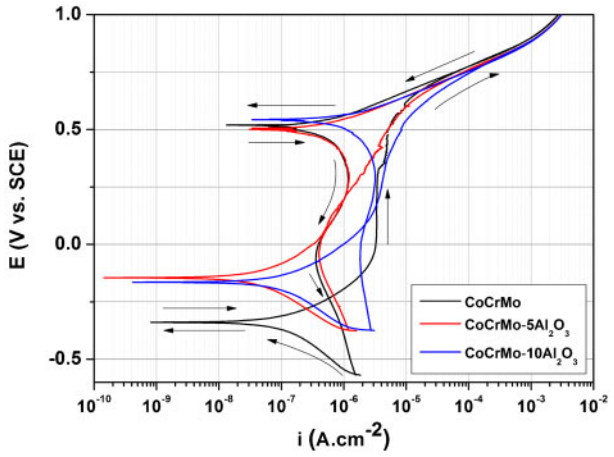

3 Polarisation curves of base CoCrMo alloy and its composites in 8 g L^{-1} NaCl solution at 37°C

corrosion potential to more noble values.[42,43] It has been reported that ceramic particle additions into a metal may increase the corrosion resistance of the base metal by the inert physical barrier role of the particles.[44,45] However, this behaviour was not clearly observed in the present study; even though first there was a small decrease and then an increase on the mean corrosion current density i_{corr} values by the particle addition, when it considered within the range of the standard deviation, no clear difference was observed between the samples (Table 4.).

The corrosion behaviour of MMCs can be significantly affected by the microstructure and composition of the matrix material, the reinforcement phase, microcracks, residual stresses, microcrevices, porosity, secondary phase precipitates and interfacial products.[46–49] The main causes of the corrosion in MMCs are reported as galvanic coupling between the matrix and the reinforcement materials, selective corrosion at the matrix/reinforcement interface, chemical degradation of interphases and reinforcement materials and corrosion of matrix defects.[50,51] Since Al_2O_3 is an inert material, it is not expected to affect directly the corrosion behaviour by the formation of a galvanic coupling between the matrix and the reinforcement or a chemical degradation of the reinforcing material.[52] Besides, no interaction products were detected at the matrix/reinforcement interface. However, incorporation of ceramic particles can modify the matrix structure or may create some structural flaws (i.e. pores and crevices), which may have an influence on the corrosion behaviour of the composite material.[52,53] It has been reported by several authors that the pore areas close to the particle contact zones, which occur due to the uncompleted sintering process, may cause crevice corrosion.[18,54–60] However, within those studies, the reported porosity values are in the range between 8 and 50%, which is much higher than the present study (0·29–2·44%). Even though, the lack of passive plateau on the composite samples may be explained by a small contribution of the localised corrosion due to the porosity and matrix/reinforcement discontinuities. However, as it can be observed in Fig. 3, when scan is reversed, just a very small hysteresis loop was observed in all samples. Even so, localised damage was visible on corroded surfaces (Fig. 4). A similar case has also been reported by Ilevbare[61] regarding the investigation of the crevice corrosion properties of a Ni–Cr–Mo alloy. The author reported a localised attack (i.e. crevice corrosion) after microstructural investigations of the corroded samples in spite of little or no hysteresis loop observed in the polarisation curves. The author stated that the absence of a hysteresis loop is not always a confirmation that localised corrosion did not occur on a specimen. Moreover, the author explained this discrepancy on the microstructures and the curves by the fact that the localised damage was small and not very significant, especially at high potentials where transpassive dissolution of the boldly exposed surface and oxygen evolution started to dominate the contribution to the total current from the specimen. The author also stated that the hysteresis loops got more prominent as the aggressiveness of the environment increases.

Figure 4 represents the corroded surfaces of each sample after cyclic polarisation tests. It can be seen from the microstructures that the γ matrix corroded homogeneously and the σ phase appears not to be significantly affected by corrosion. On the other hand, localised corrosion becomes visible on the composite samples essentially located at pore and discontinuity sites. Moreover, it can be seen that the effect of the localised damage was more severe on the CoCrMo–$10Al_2O_3$ sample (Fig. 4*c*), as compared to the CoCrMo–$5Al_2O_3$ sample (Fig. 4*b*), which may be related to the different porosity amounts of the composites (Table 3).

Tribocorrosion behaviour

The evolution of the OCP with time before, during and after the sliding is given in Fig. 5 for the unreinforced alloy and the composites, together with the coefficient of friction (COF) values obtained during the sliding. Before sliding, the OCP values were stable in all samples due to the presence of a passive film on the sample surfaces in contact with the electrolyte.[62] When the sliding started, a sudden drop on OCP values were observed for all samples due to the damaging of the passive film by the counter material.[63] During the sliding, all samples presented relatively smooth OCP evolution with a slight decrement. As general, the highest OCP values were presented by CoCrMo–$10Al_2O_3$ composites, followed by CoCrMo–$5Al_2O_3$ composites and the unreinforced alloy. These results suggest that Al_2O_3 particle addition decreased the tendency to corrosion for the HP CoCrMo alloy under the tested tribocorrosion conditions. After sliding, OCP values increased up to near the

Table 3 Porosity and hardness values

Sample	% Porosity	Hardness/HV30
CoCrMo	0·29±0·16	427±3
CoCrMo–$5Al_2O_3$	1·22±0·37	315±25
CoCrMo–$10Al_2O_3$	2·44±0·75	252±5

Table 4 Corrosion potential $E_{(i=0)}$ and corrosion current density i_{corr} values

Sample	$E_{(i=0)}$/mV	i_{corr}/×10^{-8} A cm^{-2}
CoCrMo	−293±66	9·17±4·85
CoCrMo–$5Al_2O_3$	−156±12	7·54±5·55
CoCrMo–$10Al_2O_3$	−132±87	13·07±5·18

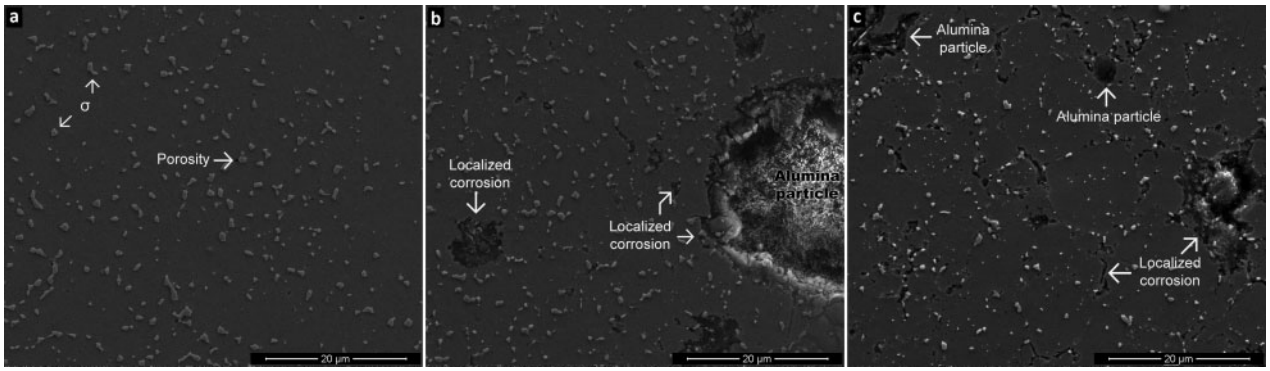

4 Secondary electron images of corroded surfaces on *a* CoCrMo, *b* CoCrMo–5Al_2O_3 and *c* CoCrMo–10Al_2O_3 samples

initial values recorded before the sliding action due to the recovering of the passive film.[30]

Figure 6 represents the low magnification SEM images of the worn surfaces for each sample. As can be seen on the images, as particle volume fraction increased, wear tracks presented smoother surface due to the load carrying effect of the ceramic particles.[28] On the other hand, particle addition resulted with relatively lower COF values on the composites (Fig. 5), which may be attributed to an increased ceramic–ceramic contact and decreased adhesive and abrasive action between the sliding surfaces. Thus, decreased tendency to corrosion on the composite samples under sliding can be explained by the decreased damage on the passive film due to the load carrying effect of the reinforcing particles, together with the effect of diminished surface area as explained for the corrosion behaviour in static conditions.

The wear behaviour of unreinforced HP CoCrMo alloy has previously been reported by some of the present authors both under dry sliding and tribocorrosion conditions with the identical tribological and electrochemical parameters that are used in the present study. After microstructural investigations and elemental analysis of the worn surfaces, the wear mechanism has been suggested as a combination of abrasive and adhesive wear for both dry sliding and tribocorrosion conditions.[27] Figure 7 represents the detailed view of the wear tracks for both composite samples together with the worn surface image and EDS analysis of the Al_2O_3

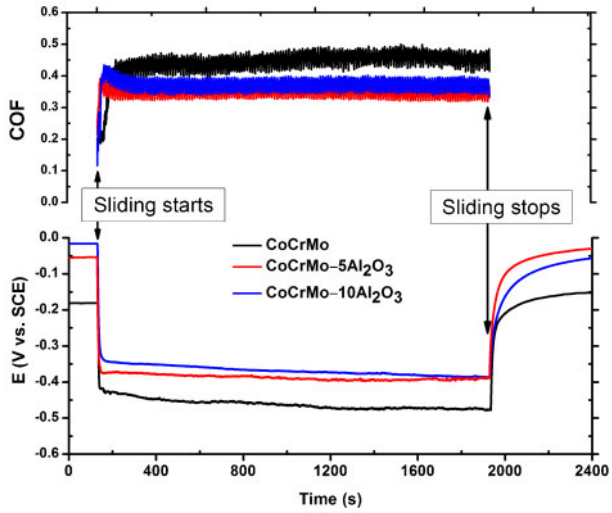

5 Evolution of OCP together with COF values during sliding

ball (counter material). Parallel sliding grooves were observed in both composite samples, and Co, Cr and Mo elements were detected by EDS analysis on both counter surfaces (Fig. 7*c*; similar morphology and analysis were obtained for both alumina ball worn against both composites). Thus, similar to the unreinforced HP CoCrMo alloy, the wear mechanism after tribocorrosion may also be suggested as mainly abrasive and adhesive wear for the composite samples.

Figure 8 presents the wear rates for each sample after the tribocorrosion tests. Although the composite samples presented lower COF values and smoother worn surfaces, an improvement was not observed on the composites in terms of wear rate. When the values are considered together with the standard deviation values, even though no significant difference was observed between the samples, the composite samples presented slightly higher mean values as compared to the unreinforced alloy.

Matrix/reinforcement interfaces have a very strong influence on the properties of the composites since there is a discontinuity in chemical composition, elastic modulus, coefficient of thermal expansion, thermodynamic properties, etc.[64] Interface characteristics and interface bonding between ceramic reinforcement and metallic matrix is also very important for the tribological properties. Depending on the bonding, the ceramic particles may protect the surface or may scoop off from the wear surface during the sliding.[28,29,65] The reason behind the wear rate values for the composite samples may be linked to the pulling out of some reinforcement particles during the sliding probably due to the lack of sufficient physical contact and eventually lack of sufficient bonding on the matrix/reinforcement interface. However, the worn surfaces of the composite samples did not present severe abrasive wear features, suggesting that pulled out particles did not create a significant third body effect. This may be attributed to the shape of the reinforcing particles that are not containing sharp edges and the relatively bigger particle size.

The as received Al_2O_3 particles that are used in the present study had a rough surface together with some contaminations of the alumina, itself (Fig. 9*a*). In order to improve the matrix/reinforcement contact, Al_2O_3 particles are cleaned to remove the contaminations (Fig. 9*b*). However, interface voids were still observed on the composite samples. Figure 9*c* represents an Al_2O_3 particle in the cross-sectional matrix structure schematically. During the cutting for sample preparation, Al_2O_3 particle can be cut from near the uppermost

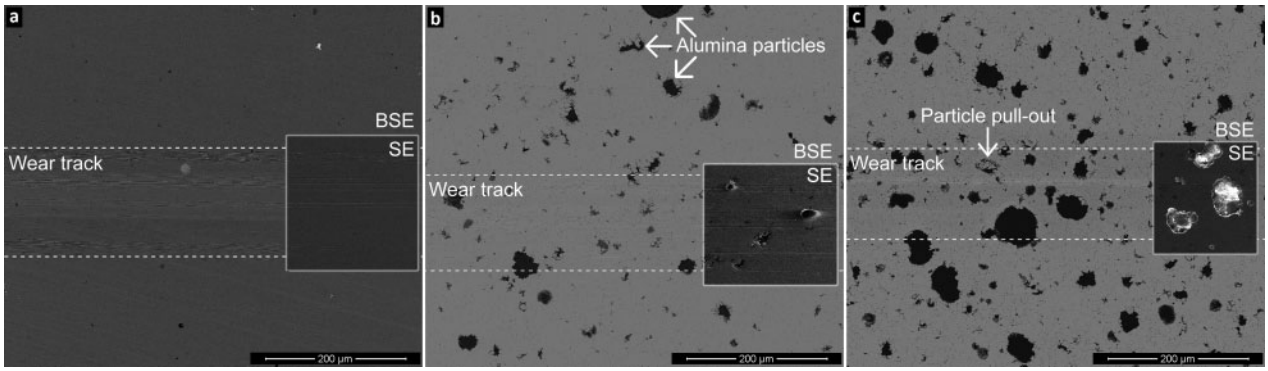

6 Low magnification SEM images of worn surfaces for *a* CoCrMo, *b* CoCrMo–5Al_2O_3 and *c* CoCrMo–10Al_2O_3 samples

part of the particle (line 1 in Fig. 9*c*), between uppermost and the middle part of the particle (line 2 in Fig. 9*c*), from the middle part of the particle (line 3 in Fig. 9*c*) or between middle and the bottom part of the particle (represented at line 4 in Fig. 9*c* as a condition as close to the bottom part of a particle). The line 3 in Fig. 9*c* is the most suitable case to observe the interfacial gaps clearly. If the cut is from line 1, the interface voids

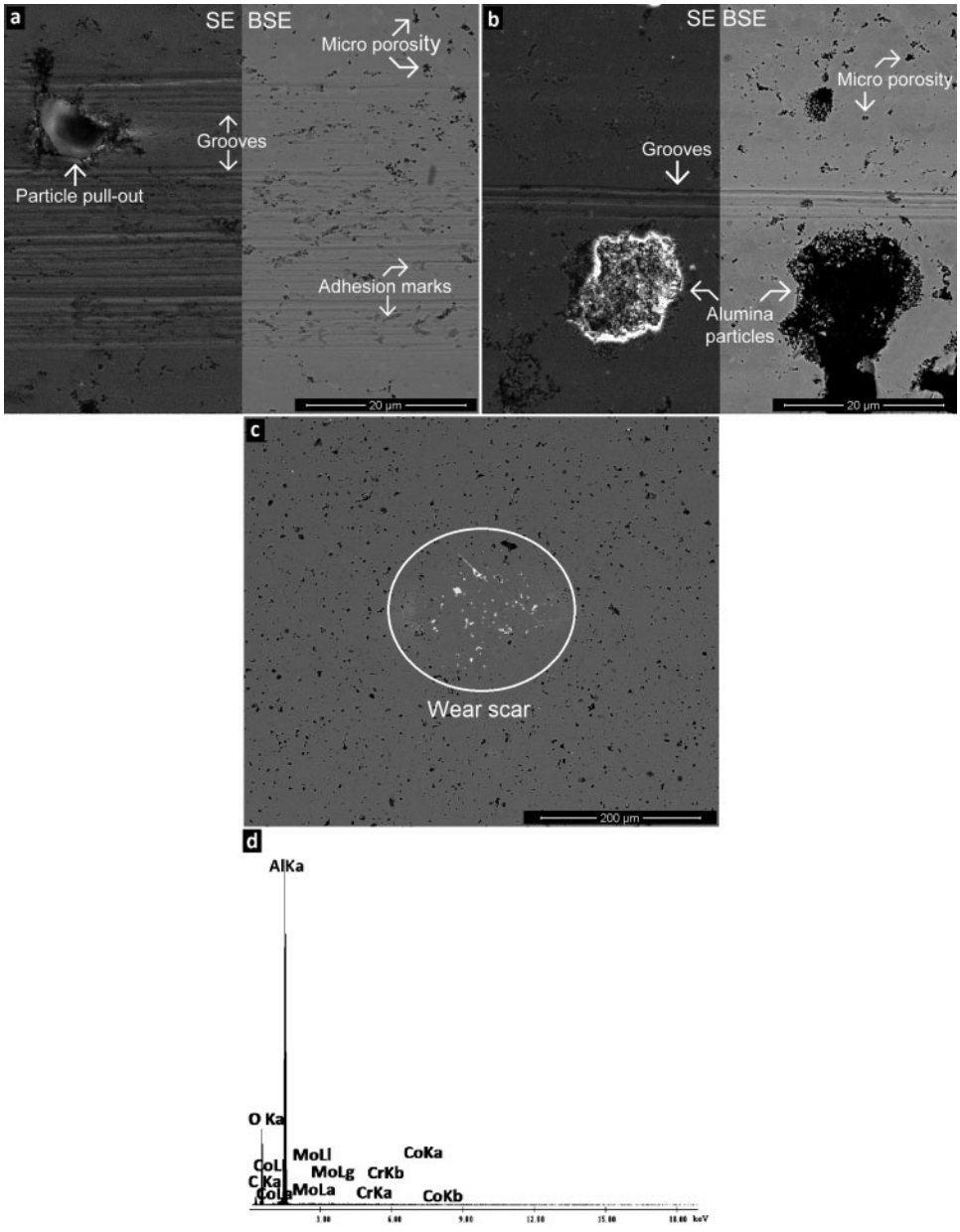

7 Detailed SEM images from wear tracks of *a* CoCrMo–5Al_2O_3 and *b* CoCrMo–10Al_2O_3 composites, *c* BSE SEM image of Al_2O_3 ball worn against CoCrMo–5Al_2O_3 sample and *d* EDS analysis taken from wear scar

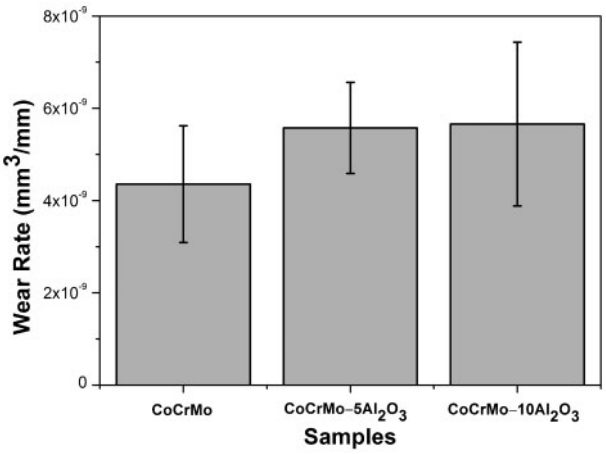

8 Wear rates after tribocorrosion tests

will be just under the surface and, therefore, may be suitable sites for localised corrosion, as well as possibility of having lack of particle support during sliding (an example can be seen on Fig. 7*b*). In case of line 2, during cutting and polishing, metallic matrix can be smeared over the ceramic particles, which may be resulted from the closure of the interface gaps (Fig. 5*c*).[66,67] Finally, in case of line 4, after the removal of the particle during cutting, the rough surface of the particle and the interface gaps may be suitable sites on the matrix for the localised corrosion (Fig. 4*b*).

Even though, it is possible to state from the microstructural investigations and electrochemical measurements that the particle pullout took place in a limited extent, which prevented catastrophic wear, as well as higher tendency to corrosion under sliding in 8 g L^{-1} NaCl solution.

Conclusion

Within the framework of this study, the followings can be concluded.

1. Microstructural investigations revealed interfacial gaps between the matrix and the reinforcement, which resulted in increased porosity on the composite samples.
2. Al_2O_3 particle addition decreased the tendency to corrosion $E_{(i=o)}$ of CoCrMo alloy. However, no significant influence was observed on the corrosion rate i_{corr}.
3. It is suggested from the microstructural investigations on the corroded surfaces and the polarisation curves that porosity induced localised corrosion took

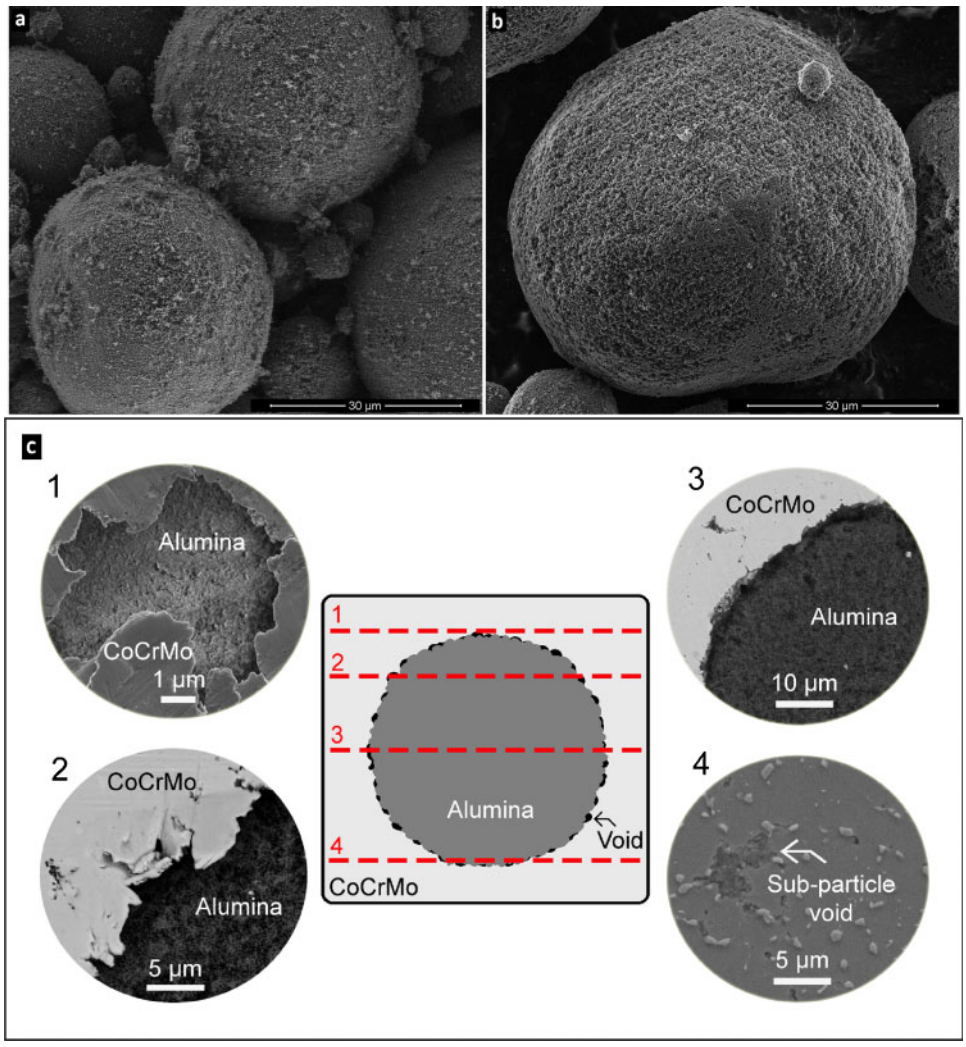

9 *a* as received, *b* as cleaned Al_2O_3 particles and *c* schematic draw of possible cutting lines for Al_2O_3 particle in cross-sectional matrix structure during sample preparation, together with representative SE (1, 4) and BSE (2, 3) SEM images from as polished (1, 3), worn (2) and corroded (4) samples

place on the composite samples. However, the localised corrosion happened in a limited extent that no hysteresis loop was observed on the cyclic polarisation curves.

4. Composite samples presented lesser tendency to corrosion under sliding in 8 g L^{-1} NaCl solution. Although composite samples presented smoother worn surfaces after tribocorrosion, an improvement was not obtained on the wear rates, which is probably related to the insufficient interface bonding between the matrix and the reinforcement.

Acknowledgements

This study was supported by the Portuguese Foundation for Science and Technology (FCT-Portugal), under project no. EXCL/EMS-TEC/0460/2012, and The Calouste Gulbenkian Foundation through 'Programa de Mobilidade Académica para Professores'. The authors also would like to thank Professor A. Ramalho (Universidade de Coimbra) for the provision of profilometry facilities.

References

1. U. I. Thomann and P. J. Uggowitzer: *Wear*, 2000, **239**, 48–58.
2. M. T. Mathew, P. Srinivasa Pai, R. Pourzal, A. Fischer and M. A. Wimmer: *Adv. Tribol.*, 2009, **2009**, 1–12.
3. Y. Yan, A. Neville and D. Dowson: *J. Phys. D*, 2006, **39D**, 3200–3205.
4. D. Landolt, S. Mischler, M. Stemp and S. Barril: *Wear*, 2004, **256**, 517–524.
5. S. K. Yen and S. W. Hsu: *J. Biomed. Mater. Res.*, 2001, **54**, 412–8.
6. I. J. Bae, O. C. Standard, G. J. Roger and D. Brazil: *J. Mater. Sci.: Mater. Med.*, 2004, **15**, 959–66.
7. L. Casabán Julián and A. Igual Muñoz: *Tribol. Int.*, 2011, **44**, 318–329.
8. F. Contu, B. Elsener and H. Böhni: *Corros. Sci.*, 2005, **47**, 1863–1875.
9. B. Vamsi Krishna, W. Xue, S. Bose and A. Bandyopadhyay: *Acta Biomater.*, 2008, **4**, 697–706.
10. M. N. Rahaman, A. Yao, B. S. Bal, J. P. Garino and M. D. Ries: *J. Am. Ceram. Soc.*, 2007, **90**, 1965–1988.
11. C. Díaz, J. A. García, S. Mändl and R. J. Rodríguez: *IEEE Trans. Plasma Sci.*, 2011, **39**, 3045–3048.
12. J. Rituerto Sin, X. Hu and N. Emami: *Tribol. Mater. Surf. Interfaces*, 2013, **7**, 1–12.
13. S. Suñer, J. L. Tipper and N. Emami: *Tribol. Mater. Surf. Interfaces*, 2012, **6**, 39–52.
14. M. S. Caicedo, R. Desai, K. McAllister, A. Reddy, J. J. Jacobs and N. J. Hallab: *J. Orthop. Res.*, 2009, **27**, 847–54.
15. M. Rosso: *J. Mater. Process. Technol.*, 2006, **175**, 364–375.
16. J. N. Reddy and C. D. Chin: *J. Therm. Stresses*, 1998, **21**, 593–626.
17. M. Grądzka-Dahlke, J. R. Dąbrowski and B. Dąbrowski: *J. Mater. Process. Technol.*, 2008, **204**, 199–205.
18. Z. Oksiuta, J. R. Dabrowski and A. Olszyna: *J. Mater. Process. Technol.*, 2009, **209**, 978–985.
19. M. T. Mathew, M. J. Runa, M. Laurent, J. J. Jacobs, L. A. Rocha and M. A. Wimmer: *Wear*, 2011, **271**, 1210–1219.
20. R. A. Gil and A. I. Muñoz: *J. Mech. Behav. Biomed. Mater.*, 2011, **4**, 2090–102.
21. M. A. Arenas, A. Conde and J. J. Damborenea: *Metall. Mater. Trans. A*, 2013, **44A**, 4382–4390.
22. A. Igual Muñoz and L. Casabán Julián: *Electrochim. Acta*, 2010, **55**, 5428–5439.
23. A. I. Muñoz and S. Mischler: *J. Mater. Sci.: Mater. Med.*, 2011, **22**, 437–50.
24. P. E. Sinnett-Jones, J. A. Wharton and R. J. K. Wood: *Wear*, 2005, **259**, 898–909.
25. Y. Yan, A. Neville, D. Dowson and S. Williams: *Tribol. Int.*, 2006, **39**, 1509–1517.
26. Y. Yan, A. Neville and D. Dowson: *Wear*, 2007, **263**, 1105–1111.
27. Z. Doni, A. C. Alves, F. Toptan, J. R. Gomes, A. Ramalho, M. Buciumeanu, L. Palaghian and F. S. Silva: *Mater. Des.*, 2013, **52**, 47–57.
28. F. Toptan, A. C. Alves, I. Kerti, E. Ariza and L. A. Rocha: *Wear*, 2013, **306**, 27–35.
29. A. Velhinho, J. D. Botas, E. Ariza, J. R. Gomes and L. A. Rocha: *Mater. Sci. Forum*, 2004, **455–456**, 871–875.
30. S. Mischler: *Tribol. Int.*, 2008, **41**, 573–583.
31. J. V. Giacchi, C. N. Morando, O. Fornaro and H. A. Palacio: *Mater. Charact.*, 2011, **62**, 53–61.
32. J. A. Betancourt-Cantera, F. Sánchez-De Jesús, G. Torres-Villaseñor, A. M. Bolarín-Miró and C. A. Cortés-Escobedo: *J. Alloys Compd*, 2012, **529**, 58–62.
33. R. Rosenthal, B. R. Cardoso, I. S. Bott, R. P. R. Paranhos and E. A. Carvalho: *J. Mater. Sci.*, 2010, **45**, 4021–4028.
34. J. Segurado, C. González and J. LLorca: *Acta Mater.*, 2003, **51**, 2355–2369.
35. R. Thiraviam, T. Sornakumar and A. S. Kumar: *Int. J. Mater. Prod. Technol.*, 2008, **31**, 305.
36. H. Y. Wang, Q. C. Jiang, Y. Wang, B. X. Ma and F. Zhao: *Mater. Lett.*, 2004, **58**, 3509–3513.
37. M. Rahimian, N. Ehsani, N. Parvin and H. R. Baharvandi: *J. Mater. Process. Technol.*, 2009, **209**, 5387–5393.
38. N. Chawla and Y.-L. Shen: *Adv. Eng. Mater.*, 2001, **3**, 357–370.
39. F. Toptan, I. Kerti and L. A. Rocha: *Wear*, 2012, **290–291**, 74–85.
40. F. C. Giacomelli, C. Giacomelli and A. Spinelli: *J. Braz. Chem. Soc.*, 2004, **15**, 541–547.
41. A. W. E. Hodgson, S. Kurz, S. Virtanen, V. Fervel, C.-O. A. Olsson and S. Mischler: *Electrochim. Acta*, 2004, **49**, 2167–2178.
42. I. Garcia, A. Conde, G. Langelaan, J. Fransaer and J. P. Celis: *Corros. Sci.*, 2003, **45**, 1173–1189.
43. T. Lampke, A. Leopold, D. Dietrich, G. Alisch and B. Wielage: *Surf. Coat. Technol.*, 2006, **201**, 3510–3517.
44. Q. Feng, T. Li, H. Teng, X. Zhang, Y. Zhang, C. Liu and J. Jin: *Surf. Coat. Technol.*, 2008, **202**, 4137–4144.
45. K. H. W. Seah, M. Krishna, V. T. Vijayalakshmi and J. Uchil: *Corros. Sci.*, 2002, **44**, 917–925.
46. T. M. Yue, Y. X. Wu and H. C. Man: *J. Mater. Sci. Lett.*, 1999, **18**, 173–175.
47. J. Hu, W. Y. Chu, W. D. Fei and L. C. Zhao: *Mater. Sci. Eng. A*, 2004, **A374**, 153–159.
48. A. Pardo, M. C. Merino, S. Merino, F. Viejo, M. Carboneras and R. Arrabal: *Corros. Sci.*, 2005, **47**, 1750–1764.
49. A. Pardo, M. C. Merino, J. Rams, S. Merino, F. Viejo and M. Campo: *Oxid. Met.*, 2005, **63**, 215–227.
50. S. L. Winkler and H. M. Flower: *Corros. Sci.*, 2004, **46**, 903–915.
51. B. Bobic, S. Mitrovic, M. Babic and I. Bobic: *Tribol. Ind.*, 2009, **31**, 44–53.
52. D. J. Lloyd: *Int. Mater. Rev.*, 1994, **39**, 1–23.
53. P. P. Trzaskoma, E. Mccafferty and C. R. Crowe: *J. Electrochem. Soc.*, 1983, **130**, 1804–1809.
54. K. H. W. Seah, R. Thampuran, X. Chen and S. H. Teoh: *Corros. Sci.*, 1995, **37**, 1333–1340.
55. K. H. W. Seah, R. Thampuran and S. H. Teoh: *Corros. Sci.*, 1998, **40**, 547–556.
56. E. Otero, A. Pardo, M. Utrilla, F. Pérez and C. Merino: *Corros. Sci.*, 1997, **39**, 453–463.
57. E. Otero, A. Pardo, M. Utrilla, E. Sáenz and J. Álvarez: *Corros. Sci.*, 1998, **40**, 1421–1434.
58. J. A. Cabral-Miramontes, J. D. O. Barceinas-Sánchez, C. A. Poblano-Salas, G. K. Pedraza-Basulto, D. Nieves-Mendoza, P. C. Zambrano-Robledo, F. Almeraya-Calderón and J. G. Chacón-Nava: *Int. J. Electrochem. Sci.*, 2013, **8**, 564–577.
59. A. V. Sameljuk, O. D. Neikov, A. V. Krajnikov, Y. V. Milman and G. E. Thompson: *Corros. Sci.*, 2004, **46**, 147–158.
60. B. S. Becker and J. D. Bolton: *Powder Metall.*, 1995, **38**, 305–313.
61. G. O. Ilevbare: *Corrosion*, 2006, **62**, 340–356.
62. N. Diomidis, N. Göçkan, P. Ponthiaux, F. Wenger and J.-P. Celis: *Intermetallics*, 2009, **17**, 930–937.
63. N. Diomidis, S. Mischler, N. S. More and M. Roy: *Acta Biomater.*, 2012, **8**, 852–9.
64. N. Chawla and K. K. Chawla: 'Metal matrix composites'; 2006, Boston, MA, Kluwer Academic Publishers.
65. D. P. Mondal and S. Das: *Tribol. Int.*, 2006, **39**, 470–478.
66. X. Zhu, H. Dong and K. Lu: *Surf. Coat. Technol.*, 2008, **202**, 2927–2934.
67. A. Kilicarslan, F. Toptan and I. Kerti: *Mater. Lett.*, 2012, **76**, 11–14.